IFT20 controls LAT recruitment to the immune synapse and T-cell activation in vivo

Omar I. Vivar[a,1], Giulia Masi[b,1,2], Jean-Marie Carpier[a,c], Joao G. Magalhaes[a], Donatella Galgano[b], Gregory J. Pazour[d], Sebastian Amigorena[a,3], Claire Hivroz[a,3], and Cosima T. Baldari[b,3]

[a]Institut Curie, Paris Sciences et Lettres (PSL) Research University, INSERM, Unité 932, Immunité et Cancer, Paris, F-75248, France; [b]Department of Life Sciences, University of Siena, 53100 Siena, Italy; [c]Université Paris Descartes, Sorbonne Paris Cité, F-75005, Paris, France; and [d]Program in Molecular Medicine, University of Massachusetts Medical School, Worcester, MA 01605

Edited by Arthur Weiss, University of California, San Francisco, CA, and approved December 4, 2015 (received for review July 11, 2015)

Biogenesis of the immune synapse at the interface between antigen-presenting cells and T cells assembles and organizes a large number of membrane proteins required for effective signaling through the T-cell receptor. We showed previously that the intraflagellar transport protein 20 (IFT20), a component of the intraflagellar transport system, controls polarized traffic during immune synapse assembly. To investigate the role of IFT20 in primary CD4$^+$ T cells in vitro and in vivo, we generated mice bearing a conditional defect of IFT20 expression in T cells. We show that in the absence of IFT20, although cell spreading and the polarization of the centrosome were unaffected, T-cell receptor (TCR)-mediated signaling and recruitment of the signaling adaptor LAT (linker for activation of T cells) at the immune synapse were reduced. As a consequence, CD4$^+$ T-cell activation and proliferation were also defective. In vivo, conditional IFT20-deficient mice failed to mount effective antigen-specific T-cell responses, and their T cells failed to induce colitis after adoptive transfer to *Rag*$^{-/-}$ mice. IFT20 is therefore required for the delivery of the intracellular pool of LAT to the immune synapse in naive primary T lymphocytes and for effective T-cell responses in vivo.

CD4+ T cell | intraflagellar transport | vesicular traffic | colitis | adoptive transfer

Vesicular traffic has emerged as a central player in the assembly and function of the immune synapse (IS), the specialized interface that forms at the T-cell membrane on contact with an antigen-presenting cell (APC) bearing cognate peptide–MHC complexes. Indeed, polarized recycling of several receptors (1, 2), including the T-cell receptor (TCR) (3), has been shown to control the clustering of these receptors at the synaptic zone and to sustain signaling initiated by their engagement. It is now well established that vesicular traffic to the IS is coopted not only by receptors but also by membrane-associated signaling mediators that are required for signal initiation and amplification, the most prominent being the kinase Lck and the adaptor LAT (linker for activation of T cells) (4, 5). These molecules are carried to the IS by recycling endosomes that move along microtubular tracks toward the centrosome, which polarizes just below the IS on contact with the cognate APC (6).

We have recently provided evidence that the intraflagellar transport protein 20 (IFT20) (7) and other components of the intraflagellar transport (IFT) system, which regulates the assembly of the primary cilium (8), act as unconventional players in IS assembly by selectively controlling the polarized traffic of recycling TCRs and other recycling receptors, such as the transferrin receptor (TfR) (9, 10). We investigate here the role of IFT20 in T-cell activation, using a conditional knockout mouse carrying a null IFT20 allele in T cells. We show that IFT20 is required for TCR signaling, IS formation, and recruitment to the TCR activation sites of vesicular LAT downstream of centrosome polarization. These defects in TCR-induced signaling of IFT20-deficient T lymphocytes translate to an inability to mount an antigen-specific T-cell response both ex vivo and in vivo. We also provide evidence of the physiological relevance of these findings by showing that IFT20 deficiency affects disease severity and outcome in a mouse model of CD4$^+$ T-cell-driven colitis.

Results and Discussion

IFT20 Controls TCR-Induced Signaling. We previously reported that IFT20 regulates vesicular trafficking to the IS in human T cells (9, 10). To achieve insights into the role of IFT20 in T cells in vivo, we crossed transgenic mice expressing the Cre recombinase under the control of a CD4 minigene with mice in which the *Ift20* locus was flanked by *loxP* sites upstream of exon 2 and downstream of exon 3 (11) (Fig. 1*A*). This strategy led to a complete loss of IFT20 expression in CD4$^+$ T cells (Fig. 1*B*). The percentages and numbers of DP and CD4$^+$ or CD8$^+$ T cells in the thymus were normal (Fig. 1*C* and Fig. S1*A*), suggesting there was no gross perturbation in T-cell development, in agreement with a recent report (12). The percentages and numbers of CD4$^+$/TCRβ$^+$ T cells in blood, lymph nodes (LN), spleen, and bone marrow were also normal, showing that IFT20 deficiency affects neither CD4$^+$ T-cell egress from the thymus nor their homeostasis in the periphery (Fig. 1*C* and Fig. S1*A*). Finally, the percentages and numbers of CD62L$^+$/CD44$^-$ (naive), CD62L$^+$/CD44$^+$ (central memory), and CD62L$^-$/CD44$^+$ (effector memory) were comparable in IFT20$^{+/+}$ and IFT20$^{-/-}$ CD4$^+$ T cells purified from bone marrow, spleen, and blood (Fig. 1*C* and Fig. S1*B*), suggesting peripheral T-cell differentiation was normal.

Significance

The immune synapse (IS), the site of cell–cell contact between T cells and antigen-presenting cells, plays a crucial role in the mounting of an immune response. Although IFT20 (intraflagellar transport protein 20), a component of the intraflagellar transport system, regulates polarized traffic to the IS, its role in T-cell activation in vivo is unknown. Here we show that in the absence of IFT20, T-cell receptor (TCR)-mediated signaling and recruitment of the signaling adaptor LAT to the immune synapse are impaired, leading to defective CD4$^+$ T-cell activation and proliferation. IFT20-defective mice fail to mount effective antigen-specific T-cell responses, and their T cells do not induce disease in a T-cell-adoptive transfer model of colitis.

Author contributions: O.I.V., G.M., J.-M.C., S.A., C.H., and C.T.B. designed research; O.I.V., G.M., J.-M.C., J.G.M., and D.G. performed research; G.J.P. contributed new reagents/analytic tools; O.I.V., G.M., J.-M.C., J.G.M., D.G., S.A., C.H., and C.T.B. analyzed data; and O.I.V., G.M., S.A., C.H., and C.T.B. wrote the paper.

The authors declare no conflict of interest.

This article is a PNAS Direct Submission.

[1]O.I.V. and G.M. contributed equally to this work.

[2]Present address: Sir William Dunn School of Pathology, University of Oxford, Oxford, OX1 3RE, United Kingdom.

[3]To whom correspondence may be addressed. Email: cosima.baldari@unisi.it, sebastian.amigorena@curie.fr, or claire.hivroz@curie.fr.

This article contains supporting information online at www.pnas.org/lookup/suppl/doi:10.1073/pnas.1513601113/-/DCSupplemental.

www.pnas.org/cgi/doi/10.1073/pnas.1513601113

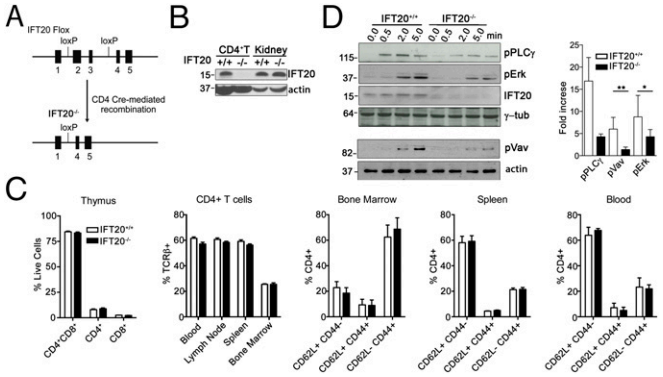

Fig. 1. TCR signaling is impaired in IFT20-deficient mice. (*A*) Mice containing LoxP sites in introns 1 and 3 were crossed to *CD4-Cre* mice generating T-cell-specific IFT20-deficient mice. (*B*) Western blot showing IFT20 expression in lysates of $CD4^+$ T cells and kidney as negative control (representative of $n = 5$). (*C*) Mean percentages of lymphocyte populations from adult $IFT20^{+/+}$ or $IFT20^{-/-}$ mice analyzed by FACS. Data compiled from three experiments ($n = 9$). (*D*) Immunoblot analysis of $IFT20^{+/+}$ and $IFT20^{-/-}$ naive $CD4^+$ T cells unstimulated (0.0) or activated with α-CD3 and α-CD28 mAbs (1 μg/mL) for the indicated times. The histogram shows the quantification of the 0- and 5-min points. Data are normalized to the loading control and presented as fold-induction of phosphorylation in response to $CD3^+CD28$ stimulation (mean ± SEM) ($n \geq 3$). Statistical significance was calculated using a ratio paired *t* test. $^*P < 0.05$; $^{**}P < 0.01$.

However, stimulation of IFT20-deficient $CD4^+$ T cells by $CD3^+CD28$-specific mAbs led to a reduced induction of phosphorylation of PLC-γ1 (phospholipase C γ), Vav, and the MAPKs (mitogen-activated protein kinase) Erk1/2 (extracellular signal-regulated kinase) compared with control littermate T cells (Fig. 1*D*). Similarly, TCR-induced signaling, namely, phosphorylation of Zap70, Vav, and LAT, was found to be impaired in Jurkat T cells silenced for IFT20 (Fig. 2*A*). These results confirm and extend our previous results obtained in human primary T cells, as well as Jurkat T cells (9), by showing that IFT20 is required for early signaling in primary murine T lymphocytes. The defect in TCR triggering reported here may be attributed to the role of IFT20 in endosome recycling. Indeed, IFT20 deficiency has been shown to affect TCR and TfR recycling (9, 10), and might similarly affect recycling of signaling molecules that control early TCR triggering.

IFT20 Controls the Recruitment of LAT to TCR Activation Sites. Given the observed impairment of TCR-mediated signaling, we next analyzed the recruitment and activation of Zap70, a tyrosine kinase essential for TCR signaling (13), at the IS of IFT20-deficient T cells. For these experiments, we used T cells purified from *Ift20*$^{fl/fl}$*CD4-Cre* mice crossed with OTI or OTII mice, which express a transgenic TCR specific for peptides derived from hen ovalbumin (OVA) in the context of $H2K^b$ or $I\text{-}A^b$, respectively. Phospho-Zap70 (pZap70; phosphorylated-ζ-chain–associated protein kinase) recruitment to the IS was analyzed by confocal microscopy in $CD4^+$ T lymphocytes incubated with LPS-matured bone marrow-derived dendritic cells (BMDC) pulsed with the specific OVA peptides. The enrichment in pZap70 at the T-cell:APC contact area was reduced for both OTI/*IFT20*$^{-/-}$ and OTII/*IFT20*$^{-/-}$ T cells (Fig. 3*A*),

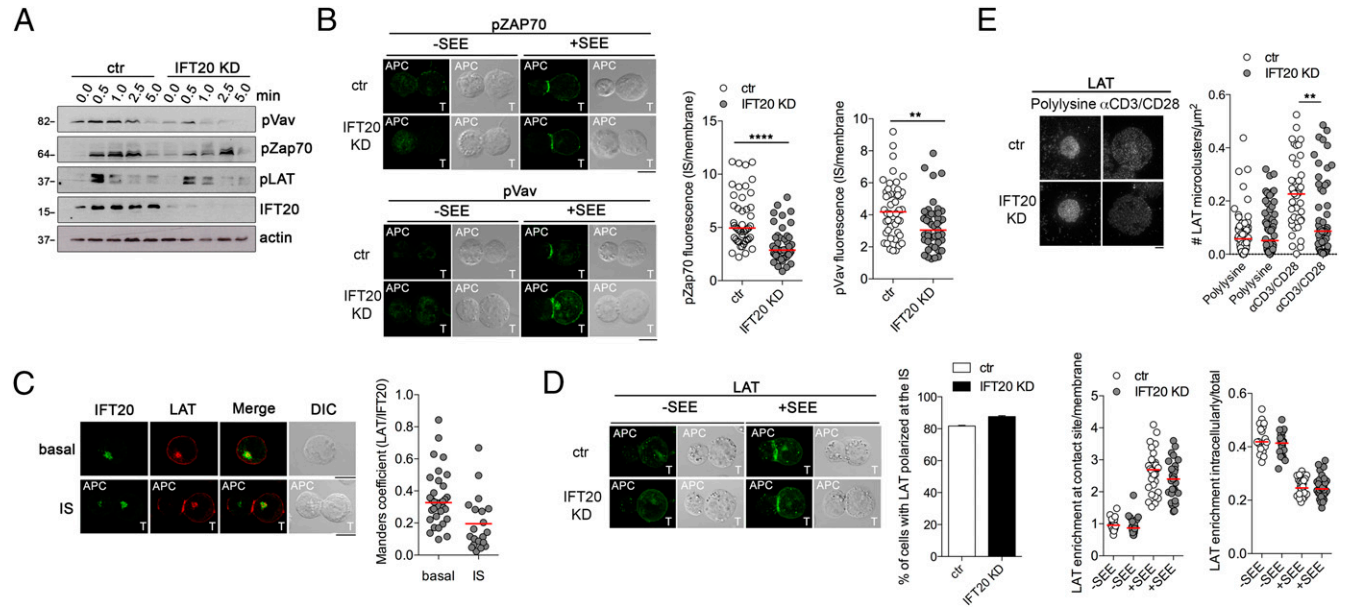

Fig. 2. Deficiency of IFT20 inhibits intracellular LAT recruitment to TCR activation sites while not affecting membrane LAT clustering at the IS. (*A*) Immunoblot analysis of control (ctr) and IFT20 KD Jurkat cells, unstimulated (0.0) or activated for the indicated time with α-CD3 and α-CD28 mAbs (1 μg/mL). Quantifications are shown in Fig. S2. A representative experiment is shown ($n \geq 3$). (*B*) Confocal micrographs showing pZap70 and pVav recruitment to the IS in conjugates of control (ctr) or IFT20 KD Jurkat cells and Raji cells either unpulsed or pulsed with staphylococcal enterotoxin E (SEE). The graphs on the right show the relative pZap70 and pVav fluorescence at the T-cell:APC contact site. The red bars indicate the median for each data set. Measurements were taken on 50 conjugates from four independent experiments. (Scale bar, 10 μm.) (*C*) Quantification using Mander's coefficient of the weighted colocalization of LAT with IFT20 in Jurkat cells, either as such or after conjugation with SEE-pulsed Raji cells. The red bars indicate the median for each data set. At least 20 cells were analyzed ($n \geq 2$). (Scale bar, 10 μm.) (*D*) Confocal micrographs showing LAT recruitment to the IS in conjugates of control (ctr) or IFT20 KD Jurkat cells and Raji cells either unpulsed or pulsed with SEE. The graphs show the percentage of conjugates harboring LAT at the IS (mean ± SEM) (*Right*) and the relative LAT fluorescence at the T-cell:APC contact site and in the intracellular pool (*Lower Right* and *Left*). The red bars indicate the median for each data set. Measurements were taken on 30 conjugates from two independent experiments. (Scale bar, 10 μm.) (*E*) TIRF analysis of the recruitment of LAT microclusters to the interface between coverslips coated with α-CD3 and α-CD28 mAbs and ctr and IFT20 KD Jurkat cells (*Left*). The single cell graph shows the number of LAT microclusters/μm^2. The red horizontal bars indicate the median for each data set ($n = 2$). Statistical significance was calculated using a nonparametric unpaired *t* test; $^{**}P < 0.01$. (Scale bar, 10 μm.)

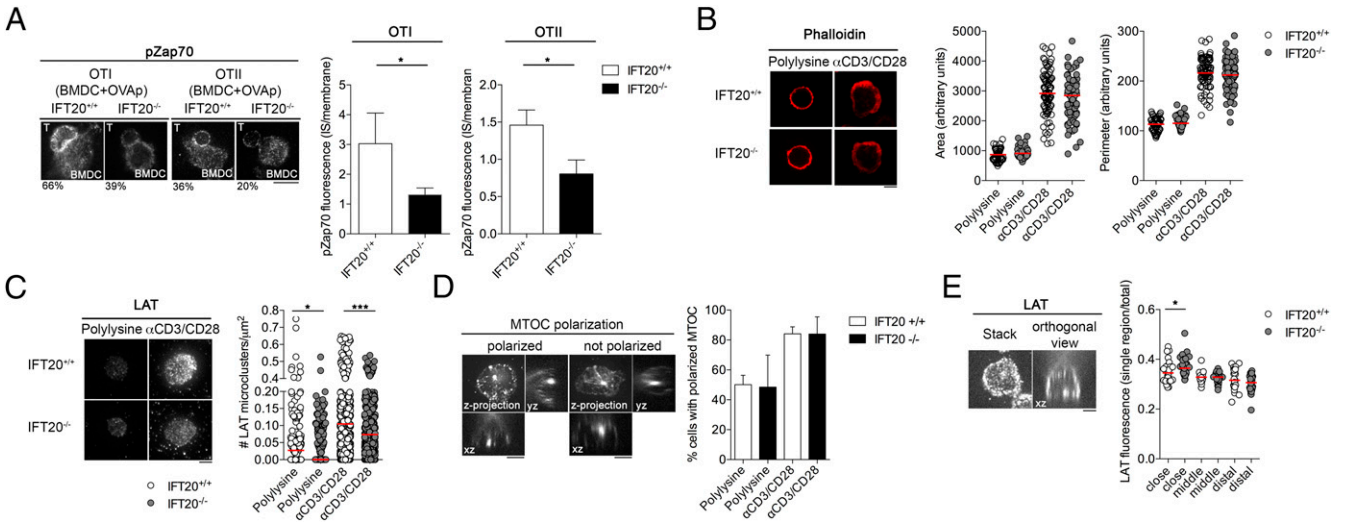

Fig. 3. Impaired recruitment of LAT and pZap70 to TCR activation sites in IFT20$^{-/-}$ CD4$^+$ T cells. (*A*) Confocal micrographs of conjugates of IFT20$^{+/+}$ and IFT20$^{-/-}$ naive CD4$^+$ T cells and BMDC preloaded with OVA peptide. Conjugates were stained with a pZap70 (p-Y493)-specific antibody. The histograms show the ratio of pZap70 fluorescence intensity at the IS compared with the rest of the membrane (mean ± SEM), quantified using ImageJ, whereas the percentages of cells showing pZap70 recruitment to the IS are indicated below the representative images (number of conjugates; OTI: WT = 33, KO = 48; OTII: WT = 54, KO = 47). (Scale bar, 10 μm.) (*B*) Confocal micrographs of IFT20$^{+/+}$ and IFT20$^{-/-}$ naive CD4$^+$ T cells plated on coverslips coated with α-CD3 and α-CD28 mAbs or poly-L-lysine as negative control. Cells were stained with phalloidin Alexa-546, and the spreading area and perimeter were measured with ImageJ and presented as arbitrary units (*Right*). The red horizontal bars indicate the median for each data set ($n = 2$). (Scale bar, 10 μm.) (*C*) TIRF micrographs showing the recruitment of LAT microclusters to the interface between coverslips coated with α-CD3 and α-CD28 mAbs and IFT20$^{+/+}$- and IFT20$^{-/-}$-naive CD4$^+$ T cells (*Left*). Single-cell graphs representing the number of LAT microclusters/μm^2 are shown on the right. The red horizontal bars indicate the median for each data set ($n = 3$). Statistical significance was calculated using an unpaired nonparametric *t* test; $*P < 0.05$; $***P < 0.005$. (Scale bar, 10 μm.) (*D*) Confocal micrographs shown as z-projections and orthogonal views of IFT20$^{+/+}$ and IFT20$^{-/-}$ naive CD4$^+$ T cells plated on coverslips coated with α-CD3 and α-CD28 mAbs and stained with an anti-α tubulin Ab (*Top*). Cells were scored on the basis of the polarization of the MTOC to the coverslip and classified as polarized or not polarized, depending on the position of the MTOC (*Bottom*). Data are presented as mean ± SD ($n = 3$). (Scale bar, 10 μm.) (*E*) Confocal micrographs shown as single stack and xz orthogonal view from the z-stack of naive CD4$^+$ T cells plated on coverslips coated with α-CD3 and α-CD28 mAbs and stained with an anti-LAT Ab (*Left*). LAT intensity was measured in three regions with the same area classified as close, middle, and distal to the coverslip. Data are expressed as ratio between LAT intensity in each area and the total LAT intensity of the cell. The red horizontal bars indicate the median for each data set ($n = 2$). Statistical significance was calculated using an unpaired nonparametric *t* test. $*P < 0.05$. (Scale bar, 10 μm.)

showing that IFT20 expression controls antigen-specific signaling at the IS. Similar results were obtained when pZap70 and pVav recruitment to the IS was analyzed on Jurkat IFT20KD cells (Fig. 2*B*).

IS formation is accompanied by T-cell spreading resulting from actin remodeling (14). To analyze this event, IFT20$^{-/-}$ CD4$^+$ T cells were incubated on coverslips coated with CD3$^+$CD28-activating mAbs or poly-L-lysine as control. F-actin was labeled with fluorescent phalloidin, and the cell area and perimeter were measured using Image J software. Activation by CD3$^+$CD28-specific mAbs induced spreading of T cells compared with poly-L-lysine. No defect in spreading was observed in IFT20-deficient CD4$^+$ T cells (Fig. 3*B*).

LAT, a key adaptor protein involved in T-cell development and activation (15, 16), has been shown to be present not only at the plasma membrane but also in subsynaptic vesicles that are rapidly recruited to activation sites in T lymphocytes (17–19). LAT has also been shown to partially colocalize with the TfR, strongly suggesting it undergoes recycling (5). Given the role of IFT20 in TfR recycling (10), we studied the relative localization of IFT20 and LAT. Confocal imaging of Jurkat cells costained for LAT and IFT20 showed a significant colocalization of IFT20 with the vesicular pool of LAT (Fig. 2*C*), which decreased after IS assembly, raising the possibility that IFT20 may be involved not only in TCR and transferrin receptor recycling (9, 10) but also in the traffic of vesicular LAT. To measure LAT recruitment, we incubated CD4$^+$ T cells on coverslips coated with CD3$^+$CD28-activating mAbs, or poly-L-lysine as control, and performed total internal reflection fluorescence microscopy (TIRFM) on cells fixed and labeled with anti-LAT Abs, as previously described (19). We observed a significant reduction in LAT recruitment to the TCR activation sites in IFT20$^{-/-}$ CD4$^+$ T cells, as shown by the lower density of LAT microclusters in the evanescent field (Fig. 3*C*). This was not a result of defective expression of CD3 or CD28 by these cells, as assessed by flow cytometry (Fig. S1*C*).

Recruitment of the intracellular pool of LAT, which is triggered by the TCR and requires several signaling mediators, including LAT itself (5), is controlled by centrosome polarization (20). We measured the polarization of the centrosome toward the coverslips in wild-type and IFT20$^{-/-}$ CD4$^+$ T cells in the same experimental setting used for the analysis of LAT recruitment. No defect in centrosome polarization to the IS was observed in IFT20$^{-/-}$ CD4$^+$ T cells (Fig. 3*D*), similar to our previous observation on human T cells (7). This indicates that the signals triggered by the TCR in IFT20$^{-/-}$ T cells, although less robust than the signals triggered in wild-type T cells (Fig. 1*D*), are sufficient to promote centrosome translocation.

Of note, when the recruitment of LAT was quantified on confocal orthogonal images of the same slides used for TIRFM, no defect of polarization of LAT in the third of the cell nearest to the activating slide was observed in the IFT20$^{-/-}$ CD4$^+$ T cells (Fig. 3*E*). Confocal imaging of IFT20-depleted Jurkat cells conjugated to staphylococcal enterotoxin E (SEE)-pulsed Raji cells showed that LAT (which, as a result of the resolution limits of this type of analysis, was likely to include both plasma membrane LAT and subsynaptic LAT$^+$ vesicles) was normally mobilized to the IS (Fig. 2*D*). However, similar to mouse primary IFT20$^{-/-}$ T cells, recruitment of LAT measured by TIRFM was decreased in IFT20-depleted Jurkat cells activated on slides

coated with anti-CD3+CD28 Abs (Fig. 2*E*). Taken together with the colocalization of IFT20 with vesicular LAT (Fig. 2*C*), these results suggest that IFT20 regulates the last step of traffic of the vesicular pool of LAT that is normally polarized in IFT20-deficient T cells but does not reach or does not dock to the plasma membrane in the synaptic zone.

Collectively, these results show that IFT20 acts as a central regulator of IS formation in primary $CD4^+$ T cells by affecting essential events triggered by the TCR downstream of centrosome polarization, which can be accounted for not only by the defect in polarized TCR recycling reported previously (9, 10) but also by a defect in the traffic of vesicular LAT to the TCR activation sites.

IFT20 Controls ex Vivo Activation of T Lymphocytes. To next address the potential role of IFT20 in T-cell activation, $CD4^+$ T cells were purified from spleens and LNs and activated ex vivo, using different concentrations of $CD3^+CD28$-specific mAbs.

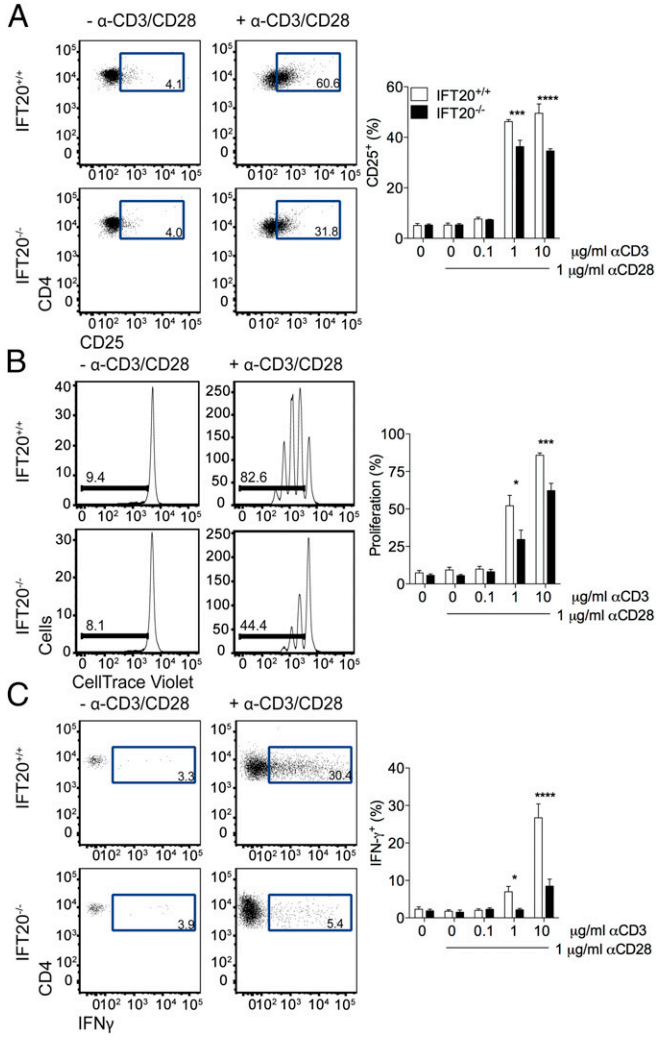

Fig. 4. Impaired activation of $CD4^+$ T cells in vitro. (*A*) CD25 expression was analyzed by FACS after 20 h of culture of total $CD4^+$ T cells isolated from spleens and LNs in the presence or absence of α-CD3 (10 μg/mL) and α-CD28 (1 μg/mL) mAbs (*Left*) or the indicated concentrations of α-CD3 and α-CD28 mAbs (*Right*). Cell proliferation (*B*) and IFNγ expression (*C*) were analyzed after 72 h of culture in the presence or absence of α-CD3 (10 μg/mL) and α-CD28 (1 μg/mL) mAbs (*Left*) or the indicated concentrations of α-CD3 and α-CD28 mAbs (*Right*). Error bars represent SEM ($n = 3$). Statistical significance was calculated using Student's *t* test. *$P < 0.05$; ***$P < 0.005$; ****<0.001.

Expression of CD25 (Fig. 4*A*), proliferation (Fig. 4*B*), and IFNγ production in the supernant (Fig. 4*C*) were reduced in $IFT20^{-/-}$ $CD4^+$ T cells compared with their wild-type counterparts, demonstrating that IFT20 expression is required for efficient activation of $CD4^+$ T cells.

IFT20 Controls T Cell Functions in Vivo. To test whether IFT20 controls TCR-induced T-cell activation in vivo, we first checked the T-cell response to an antigenic challenge. Lethally irradiated WT CD45.1 C57BL6 mice were reconstituted with bone marrow from CD45.2 *Ift20*$^{fl/fl}$*CD4-Cre* mice and *Ift20*$^{fl/fl}$ controls (Fig. 5*A*). Reconstitution of the T-cell compartment was comparable in chimeras generated with bone marrows from *Ift20*$^{fl/fl}$*CD4-Cre* and from *Ift20*$^{fl/fl}$ littermate controls (Fig. 5*B*). The mouse chimeras were immunized with OVA in complete Freund adjuvant, and 10 days after immunization, splenocytes were restimulated in vitro in the presence of OVA. Concentrations of cytokines present in the supernatants were measured 24 h later. Production of all cytokines tested (IL-17A, IFNγ, IL-4, TNF-α, and IL-2) was reduced in $IFT20^{-/-}$ $CD4^+$ T lymphocytes (Fig. 5*C*). The impairment in IL-17A production by $IFT20^{-/-}$ $CD4^+$ T lymphocytes after in vitro restimulation with phorbol myristate acetate (PMA)+ionomycin or OVA was confirmed by intracellular staining (Fig. 5*D*). These results show that expression of IFT20 by T cells is required for mounting a $CD4^+$ T-cell response after immunization.

To further analyze the role of IFT20 in T-cell activation, we used a T-cell-induced model of colitis. Naive $CD4^+$ T cells purified from *Ift20*$^{fl/fl}$*CD4-Cre* mice and *Ift20*$^{fl/fl}$ control littermates were transferred into C57BL6 *Rag2*$^{-/-}$ mice. In this model, the T-cell transfer in immunodeficient mice induces a chronic colitis (21). Because IL-17A was shown to be critical for T-cell-mediated colitis (22), mice were killed and $CD4^+$ T lymphocytes were purified from mesenteric LNs and activated with PMA+ionomycin to reveal their ability to produce IL-17A. The percentages of $IL\text{-}17A^+CD4^+$ T cells were lower in LNs from *Ift20*$^{fl/fl}$*CD4-Cre* mice compared with *Ift20*$^{fl/fl}$ control littermates (Fig. 5*E*). To appreciate the intestinal inflammation in the model, we measured the length of the colon. Colons from *Rag2*$^{-/-}$ mice reconstituted with $CD4^+$ T cells from control mice were significantly shorter than colons from *Rag2*$^{-/-}$ recipient mice (Fig. 5*E*). In contrast, colons from *Rag2*$^{-/-}$ mice reconstituted with IFT20-deficient $CD4^+$ T cells did not show any significant modification of their length (Fig. 5*E*). Finally, survival of the mice transferred with $IFT20^{-/-}$ $CD4^+$ T cells was not altered compared with that of control *Rag2*$^{-/-}$ mice, whereas under the same conditions, the transfer of wild-type $CD4^+$ T cells resulted in premature death of the mice or their being killed because of a weight loss of more than 20% of their initial body weight (Fig. 5*E*). Collectively, these results show that $IFT20^{-/-}$ $CD4^+$ T cells have a strongly reduced pathogenicity, which is most probably a result of their reduced production of IL-17A, and possibly other proinflammatory cytokines. Interestingly, a recent report showed that *ift20* deletion in CD4 T cells has only mild effects on the development of collagen-induced arthritis (12), another T-cell-related autoimmune disorder. Although the pattern of cytokine production was not investigated in that report, the effect of IFT20 deficiency on the development of pathogenic Th17 cells may have been underestimated in this experimental model, which involves the use of a potent adjuvant.

The data presented in this report extend and validate in vivo the role that IFT20 plays in IS assembly by regulating the traffic to the T-cell:APC interface not only of endosome-associated TCRs (9) but also of the endosomal pool of LAT, which acts as a scaffold for the assembly of multimolecular complexes that amplify TCR-generated signals. LAT is present both at the plasma membrane and in intracellular pools, which are recruited to the TCR activation sites (5, 17–19). Both pools have been shown to

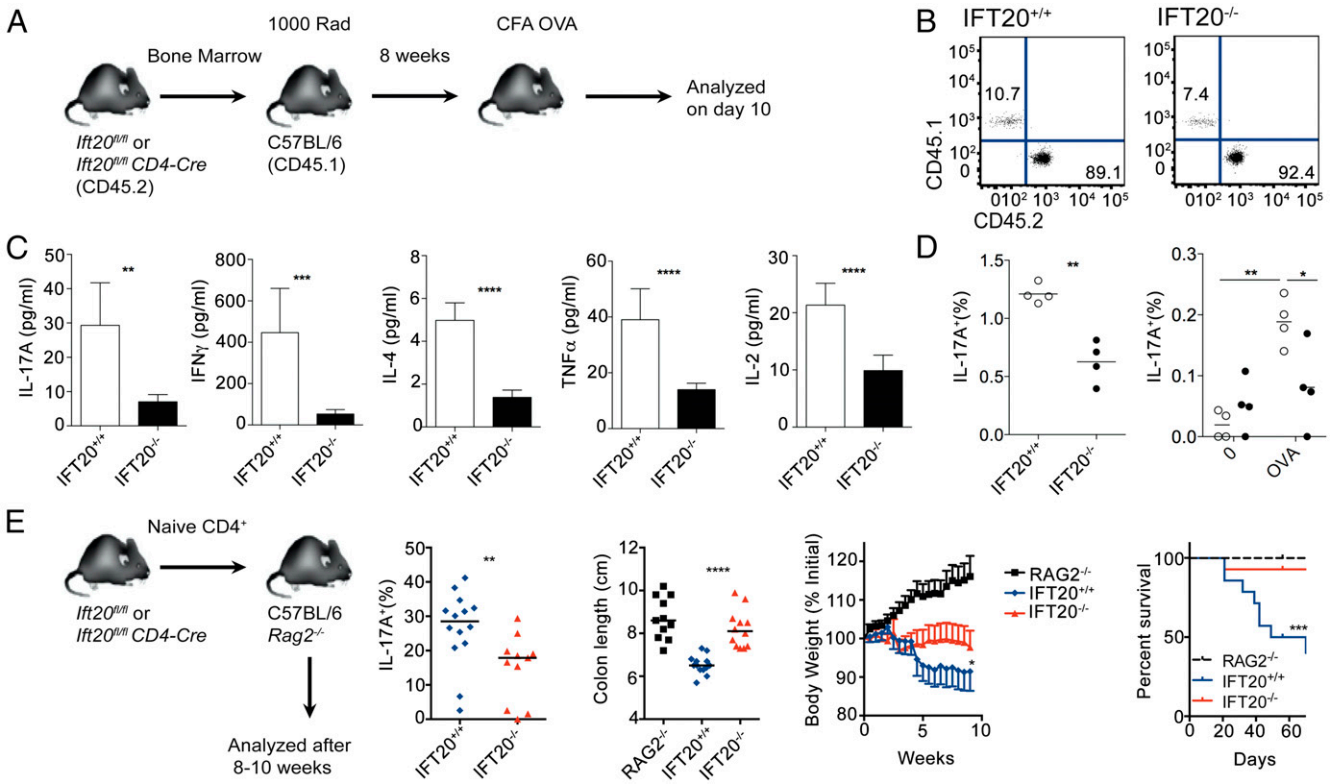

Fig. 5. Impaired CD4$^+$ T-cell response in IFT20-deficient mice. (*A*) Bone marrow (BM) chimeras were generated by reconstituting lethally irradiated WT CD45.1 mice with BM from *Ift20*$^{fl/fl}$ or *Ift20*$^{fl/fl}$*CD4-Cre* mice (CD45.2). (*B*) The ratio of CD45.1$^+$ and CD45.2$^+$ CD4$^+$ T cells in the spleens of chimeric mice in a representative experiment is shown. (*C*) Cytokine production by splenocytes from mice 10 d after immunization with complete Freund's adjuvant OVA was assessed by cytometric bead array (CBA) after 24 h of OVA restimulation. Error bars represent SEM ($n = 4$ mice; data from two experiments). (*D*) Intracellular flow cytometric analysis of total IL-17A production in CD4$^+$ cells after PMA+ionomycin restimulation (*Left*) and antigen-specific IL-17A production in CD4$^+$ T cells restimulated with OVA. The horizontal bars represent the median ($n = 4$ mice) data from two experiments. (*E*) Colitis was induced by transfer of FACS-sorted naive CD4$^+$ T cells into C57BL6 *Rag2*$^{-/-}$ mice. Mice were killed 8–10 wk after transfer or upon losing 20% of their initial body weight. IL-17A production in CD4$^+$ T cells from mesenteric LNs from mice reconstituted with IFT20$^{+/+}$ (blue diamonds) or IFT20$^{-/-}$ (red triangles) BM. Colon length at time of sacrifice of *Rag2*$^{-/-}$ mice (black squares), mice reconstituted with IFT20$^{+/+}$ (blue diamonds), or IFT20$^{-/-}$ (red triangles) BM. Percentage initial body weight of *Rag2*$^{-/-}$ mice (black squares), mice reconstituted with IFT20$^{+/+}$ (blue diamonds), or IFT20$^{-/-}$ (red triangles) BM. Survival curve of *Rag2*$^{-/-}$ mice (black dashed line), mice reconstituted with IFT20$^{+/+}$ (blue solid line) or IFT20$^{-/-}$ (red solid line) BM. Data compiled from two experiments ($n = 14$ mice per group). *$P < 0.05$; **$P < 0.01$; ***$P < 0.005$; ****$P < 0.001$. Statistical significance was calculated using Student's *t* test (*C* and *D*) or one-way ANOVA (*E*).

play a role in T-cell activation (18, 19, 23, 24). We show here that LAT fails to reach this membrane-proximal location in IFT20-deficient T cells (Figs. 2*E* and 3*C*) despite polarization of the centrosome (Fig. 3*D*). However, LAT-dependent signaling is not completely abolished, suggesting the plasma membrane pool of LAT can still signal, but the subsynaptic vesicular pool cannot.

It is worth noting that although partial, the signaling defect induces an important functional T-cell defect in vivo. Indeed, IFT20 deficiency results in a defect in the production of all the cytokines tested, including Th1, Th2, and Th17 cytokines. This result suggests the T-cell differentiation defects observed in *IFT20*$^{fl/fl}$/*CD4*^{Cre} mice are the consequence of the impaired ability of CD4$^+$ T cells to become activated in response to TCR signaling, rather than of a selective defect in their differentiation. Although we favor the explanation that the defect in TCR signaling in IFT20$^{-/-}$ T cells causes these defects in the biological response, we cannot at this stage rule out that IFT20 is implicated in the regulation of other pathways that control cytokine production. Moreover, it is possible that we underestimated the TCR signaling defect in our in vitro experiments where T lymphocytes are activated with high concentrations of anti-CD3$^+$CD28 Abs. In in vivo conditions, triggering of the TCR is likely to be much lower, thus allowing us to better reveal the functional outcome of IFT20 deficiency.

In conclusion, the results presented here show that, in primary mouse CD4$^+$ T lymphocytes, IFT20 expression is required for TCR-induced signaling, recruitment of vesicular LAT to the TCR activation sites, and CD4$^+$ T-cell function in vivo. IFT20 is a component of the IFT system that controls the assembly of the primary cilium (8). Based on our finding that a number of components that regulate this process are implicated in vesicular traffic to the IS in T cells (9, 10, 25, 26), studying the pathways that control ciliogenesis should provide new molecules implicated in IS assembly and function.

Materials and Methods

Mice, Cells, Reagents, and Antibodies. Mice with T-cell-specific deletion of IFT20 were generated by crossing *Ift20*$^{fl/fl}$ mice (11) with *CD4-Cre* mice. OTI and OTII mice were crossed to *Ift20*$^{fl/fl}$*CD4-cre* mice to obtain *Ift20*$^{fl/fl}$*CD4-Cre* OTI and *Ift20*$^{fl/fl}$*CD4-Cre* OTII mice, respectively. Further details are provided in the *SI Materials and Methods*.

Purification of naive CD4$^+$ T cells from LNs and spleens was carried out as detailed in the *SI Materials and Methods*. BMDC were differentiated as described previously (27). Details on the activation of BMDC, loading with either class I ($OVA_{257–264}$) or class II ($OVA_{323–339}$) peptide and incubation with OTI and OTII cells, respectively, are provided in the *SI Materials and Methods*.

Cell lines include Jurkat T cells and Raji B cells. Stable IFT20 knock-down Jurkat cells (IFT20 KD; ~70% depletion) were previously described (9).

Anti-CD3 and anti-CD28 mAbs used for T-cell activation as well as other Abs and reagents are listed in the *SI Materials and Methods*.

BM Chimeras. BM chimeras were generated as detailed in the *SI Materials and Methods*.

Immunizations. The protocol for immunization is described in the *SI Materials and Methods*.

Colitis. Colitis was induced by i.v. injection of FACS-sorted naive $CD4^+$ T cells from *ift20*$^{fl/fl}$ or *ift20*$^{fl/fl}$ *CD4-cre* donor mice into age-matched *Rag2*$^{-/-}$ recipients and scored as described in the *SI Materials and Methods*.

Flow Cytometry. The protocols for flow cytometric analysis of surface markers and intracellular cytokines are described in the *SI Materials and Methods*.

T-Cell Proliferation Assay. T-cell proliferation assays were carried out as described in the *SI Materials and Methods*.

Immunoblots. Jurkat cells and mouse $CD4^+$ T cells were processed for immunoblot as described in the *SI Materials and Methods*.

Microscopy and Image Analysis. The detailed protocols for confocal imaging and TIRF microscopy of mouse $CD4^+$ T cells and Jurkat cells are described in the *SI Materials and Methods*. TIRFM images were analyzed with ImageJ software as described (28), using the strategy detailed in the *SI Materials and Methods*.

Statistical Analysis. Unpaired Student's *t* test, unpaired nonparametric *t* test, ratio paired *t* test, and one-way ANOVA test were used for statistical analysis. SEM and *P* values were determined using Prism software.

ACKNOWLEDGMENTS. We thank V. Fraisier from the The BioImaging Cell and Tissue Core Facility of the Institut Curie (Pict IBISA) and L. Sengmanivong and the Nikon Imaging Centre @ Institut Curie-CNRS for technical assistance with microscopy and image analysis. O.I.V. was financed by the Association pour la Recherche sur le Cancer, G.M. by FISM (Fondazione Italiana Sclerosi Multipla), and J.-M.C. by la Ligue contre le Cancer. C.H. was supported by ANR-13-BSV2-0018 "NeuroImmunoSynapse" and la Fondation pour la Recherche Médicale. The financial support of Telethon-Italy (Grant GGP1102) to C.T.B. is gratefully acknowledged. G.J.P. received support from National Institutes of Health (GM060992). S.A. received funding from the Institut Curie, Institut National de la Santé et de la Recherche Médicale, Centre National de la Recherche Scientifique, Ligue Contre le Cancer (Equipe Labellisée EL2014.LNCC/SA), Association de Recherche Contre le Cancer, Grant ERC (2013-AdG No. 340046 DCBIOX), and Labex DC-BIOL. The study was also supported by ANR-10-IDEX-0001-02 PSL* and ANR-11-LABX-0043.

1. Soares H, Lasserre R, Alcover A (2013) Orchestrating cytoskeleton and intracellular vesicle traffic to build functional immunological synapses. *Immunol Rev* 256(1): 118–132.
2. Finetti F, Baldari CT (2013) Compartmentalization of signaling by vesicular trafficking: A shared building design for the immune synapse and the primary cilium. *Immunol Rev* 251(1):97–112.
3. Das V, et al. (2004) Activation-induced polarized recycling targets T cell antigen receptors to the immunological synapse; involvement of SNARE complexes. *Immunity* 20(5):577–588.
4. Ehrlich LI, Ebert PJ, Krummel MF, Weiss A, Davis MM (2002) Dynamics of p56lck translocation to the T cell immunological synapse following agonist and antagonist stimulation. *Immunity* 17(6):809–822.
5. Bonello G, et al. (2004) Dynamic recruitment of the adaptor protein LAT: LAT exists in two distinct intracellular pools and controls its own recruitment. *J Cell Sci* 117(Pt 7): 1009–1016.
6. Fooksman DR, et al. (2010) Functional anatomy of T cell activation and synapse formation. *Annu Rev Immunol* 28:79–105.
7. Follit JA, Tuft RA, Fogarty KE, Pazour GJ (2006) The intraflagellar transport protein IFT20 is associated with the Golgi complex and is required for cilia assembly. *Mol Biol Cell* 17(9):3781–3792.
8. Pedersen LB, Rosenbaum JL (2008) Intraflagellar transport (IFT) role in ciliary assembly, resorption and signalling. *Curr Top Dev Biol* 85:23–61.
9. Finetti F, et al. (2009) Intraflagellar transport is required for polarized recycling of the TCR/CD3 complex to the immune synapse. *Nat Cell Biol* 11(11):1332–1339.
10. Finetti F, et al. (2014) Specific recycling receptors are targeted to the immune synapse by the intraflagellar transport system. *J Cell Sci* 127(Pt 9):1924–1937.
11. Jonassen JA, San Agustin J, Follit JA, Pazour GJ (2008) Deletion of IFT20 in the mouse kidney causes misorientation of the mitotic spindle and cystic kidney disease. *J Cell Biol* 183(3):377–384.
12. Yuan X, Garrett-Sinha LA, Sarkar D, Yang S (2014) Deletion of IFT20 in early stage T lymphocyte differentiation inhibits the development of collagen-induced arthritis. *Bone Res* 2:14038–14049.
13. Wang H, et al. (2010) ZAP-70: An essential kinase in T-cell signaling. *Cold Spring Harb Perspect Biol* 2(5):a002279.
14. Dustin ML, Cooper JA (2000) The immunological synapse and the actin cytoskeleton: Molecular hardware for T cell signaling. *Nat Immunol* 1(1):23–29.
15. Zhang W, et al. (1999) Essential role of LAT in T cell development. *Immunity* 10(3): 323–332.
16. Zhang W, Sloan-Lancaster J, Kitchen J, Trible RP, Samelson LE (1998) LAT: The ZAP-70 tyrosine kinase substrate that links T cell receptor to cellular activation. *Cell* 92(1): 83–92.
17. Purbhoo MA, et al. (2010) Dynamics of subsynaptic vesicles and surface microclusters at the immunological synapse. *Sci Signal* 3(121):ra36.
18. Williamson DJ, et al. (2011) Pre-existing clusters of the adaptor Lat do not participate in early T cell signaling events. *Nat Immunol* 12(7):655–662.
19. Larghi P, et al. (2013) VAMP7 controls T cell activation by regulating the recruitment and phosphorylation of vesicular Lat at TCR-activation sites. *Nat Immunol* 14(7): 723–731.
20. Blanchard N, Di Bartolo V, Hivroz C (2002) In the immune synapse, ZAP-70 controls T cell polarization and recruitment of signaling proteins but not formation of the synaptic pattern. *Immunity* 17(4):389–399.
21. Griseri T, Asquith M, Thompson C, Powrie F (2010) OX40 is required for regulatory T cell-mediated control of colitis. *J Exp Med* 207(4):699–709.
22. Yen D, et al. (2006) IL-23 is essential for T cell-mediated colitis and promotes inflammation via IL-17 and IL-6. *J Clin Invest* 116(5):1310–1316.
23. Balagopalan L, Barr VA, Kortum RL, Park AK, Samelson LE (2013) Cutting edge: Cell surface linker for activation of T cells is recruited to microclusters and is active in signaling. *J Immunol* 190(8):3849–3853.
24. Soares H, et al. (2013) Regulated vesicle fusion generates signaling nanoterritories that control T cell activation at the immunological synapse. *J Exp Med* 210(11): 2415–2433.
25. Onnis A, et al. (2015) The small GTPase Rab29 is a common regulator of immune synapse assembly and ciliogenesis. *Cell Death Differ* 22(10):1687–1699.
26. Finetti F, et al. (2015) The small GTPase Rab8 interacts with VAMP-3 to regulate the delivery of recycling T-cell receptors to the immune synapse. *J Cell Sci* 128(14): 2541–2552.
27. Winzler C, et al. (1997) Maturation stages of mouse dendritic cells in growth factor-dependent long-term cultures. *J Exp Med* 185(2):317–328.
28. Tourret M, et al. (2010) T cell polarity at the immunological synapse is required for CD154-dependent IL-12 secretion by dendritic cells. *J Immunol* 185(11):6809–6818.
29. Pazour GJ, et al. (2002) The intraflagellar transport protein, IFT88, is essential for vertebrate photoreceptor assembly and maintenance. *J Cell Biol* 157(1):103–113.